Journal of Colloid and Interface Science 592 (2021) 430–439

Contents lists available at ScienceDirect

Journal of Colloid and Interface Science

journal homepage: www.elsevier.com/locate/jcis

Regular Article

Photopolymerizable pullulan: Synthesis, self-assembly and inkjet printing

Giulia Mugnaini, Claudio Resta, Giovanna Poggi, Massimo Bonini *

CSGI & Department of Chemistry "Ugo Schiff", via della Lastruccia 3, 50019 Sesto Fiorentino, FI, Italy

GRAPHICAL ABSTRACT

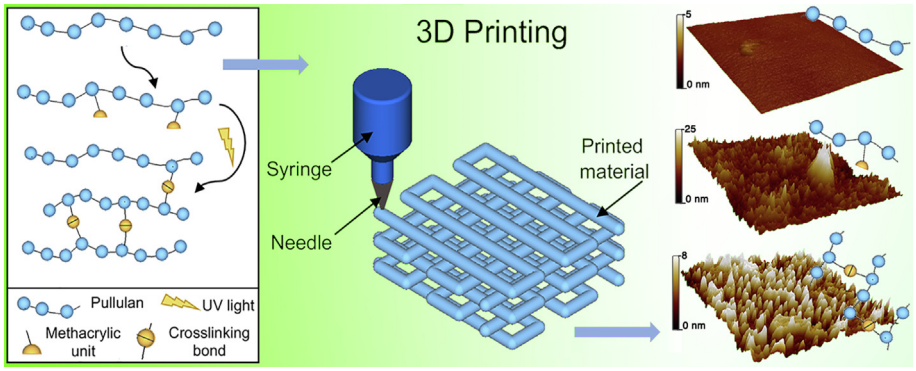

ARTICLE INFO

Article history:
Received 15 January 2021
Revised 8 February 2021
Accepted 16 February 2021
Available online 2 March 2021

Keywords:
Biopolymer
Pullulan
Photo-activated cross-linking
Printing
Rheology
Mechanical properties

ABSTRACT

Hypothesis: Pullulan, an exopolysaccharide consisting of maltotriose repeating units, has recently found many applications in different fields, such as food, packaging, cosmetics and pharmaceuticals. The introduction of photo-crosslinkable methacrylic units potentially allows to use pullulan derivative in inkjet 3D printing.

Experiments: Pullulan was functionalized with methacrylic groups and the derivative was characterized by NMR, FT-IR and Raman spectroscopy. Water dispersions were thoroughly investigated by optical microscopy, SAXS and rheology to evaluate the self-assembly properties and they were used as photo-crosslinkable inks in a 3D printer, also in comparison with pristine pullulan. The structural and mechanical properties of the obtained films were studied by Atomic Force Microscopy and tensile strength tests.

Findings: The introduction of methacrylic groups moderately affects the self-assembly of the polymer in water, resulting in a slight increase of the gyration radius of the polymer coils and in a small decrease of the viscosity, retaining the typical shear-thinning behavior of concentrated polysaccharides in water. The structural and mechanical properties of the 3D printed films are much more affected, showing the presence of sub-micrometric phase segregated domains which are further separated by the cross-linking. As a result, the deformability of the materials is improved, with a lower tensile strength.

Abbreviations: AM, Additive Manufacturing; Pul, Pullulan; DMSO, Dimethyl sulfoxide; DMF, Dimethylformamide; FDA, Food and Drug Administration; 3D, Three dimensional; 3DP, Three dimensional printing; PLA, Poly (lactic acid); ABS, Acrylonitrile-butadiene-styrene; PC, Polycarbonate; PCL, Polycaprolactone; Pul-Ma, Methacrylated pullulan; Ma, Methacrylic anhydride; EtOH, Ethanol; RT, Room temperature; FD, Functionalization degree; ^{1}H NMR, Proton nuclear magnetic resonance spectroscopy; ^{13}C NMR, Carbon nuclear magnetic resonance spectroscopy; FT-IR, Fourier transform infrared spectroscopy; ATR, Attenuated total reflectance; PCM, Phase-contrast microscopy; CCD, Charge-coupled device; SAXS, Small angle X-rays scattering; .STL, Stereolithography format file; AFM, Atomic force microscopy.

* Corresponding author.
E-mail address: massimo.bonini@unifi.it (M. Bonini).

https://doi.org/10.1016/j.jcis.2021.02.074
0021-9797/

1. Introduction

The recent progresses in additive manufacturing (AM) techniques and their exploitation in tissue engineering have imposed the need to develop new processable materials and, at the same time, to implement the properties of the materials already in use, especially in terms of the mechanical properties of the final products [1]. Among them, natural biopolymers, such as cellulose, gelatin, chitosan and pullulan, have recently attracted significant attention [2–4,5–11]. Pullulan (Pul) is a linear, non-ionic polysaccharide with chemical formula $(C_6H_{10}O_5)_n$ as obtained by elemental analysis [12,13,14,15]. First isolated and characterized from the culture broths of *Aureobasidium pullulans* in 1958 by Bernier et al. [16], its structure has been resolved by Bender and Wallenfels et al. in the beginning of '60s [17,18]. Its structure consists of maltotriose repeating units (*i.e.,* three glucose molecules linked by α (1 → 4) glycosidic bonds) connected by α (1 → 6) glycosidic bonds [13,14,15]. At room temperature pullulan is a white dry, tasteless and odorless, non-hygroscopic powder [13,19,15]. Thanks to its unique chemical structure, pullulan is highly soluble in water, but insoluble in almost any organic solvents except for dimethyl sulfoxide (DMSO) and dimethylformamide (DMF) [20,13,14]. It shows a good thermal stability (decomposing over 250 °C [13,19,15]) and its aqueous solutions are stable in a wide pH range [13,14], displaying a lower viscosity with respect to other polysaccharides and not showing the tendency to form gel phases [13,14,21], suggesting weak intermolecular interactions in water. Pullulan peculiar structure provides adhesive and oxygen barrier properties [13] and the ability to be molded into different shapes [14,19,15] and to form fibers and thin films [13,15,19]. Thanks to these properties, pullulan finds potential applications in food industries, as coating for food-packing [19,22,23] or stabilizer and emulsifiers for food products [14], and in the pharmaceutical field [24]. Moreover, it is one of the FDA (Food and Drug Administration) approved biopolymers since it is biodegradable, non-toxic, bio- and hemo-compatible, non-mutagenic, non-carcinogenic, non-immunogenic [13,19,25,26].

Pullulan also represents a good candidate for introduction of new chemical functionalities along the backbone to modify its chemical and/or physical properties and eventually extend its applications. Thanks to the presence of nine hydroxyl groups on each monomeric unit, pullulan can be involved in many different chemical reactions [14] such as esterification [27,28], oxidation [29,30,31], etherification [32,33], copolymerization [34,35,36], sulfonation [37] and chlorination [38]. The introduction of monomers, such as acrylates and methacrylates, is a viable strategy for the preparation of chemically cross-linked polymeric hydrogels [39], also in the case of biopolymers [40] and polysaccharides [41,42]. For this purpose it is possible to use a two-step process where reactive double bonds are first introduced along the polymer chain and, in a second step, used to crosslink the chains by a free radical polymerization process [43].

In the last few years, pullulan has become an interesting material for different biomedical applications, including its use as a carrier for drugs [44] and gene delivery [14,15] and its exploitation for the construction of scaffolds for tissue engineering [15,45,46]. In particular, pullulan and its derivatives are promising candidates as inks in three-dimensional printing (3DP) processes for the construction of synthetic scaffolds or transdermal patches [47,48]. 3DP has become a very popular technique to create three-dimensional (3D) structures for its ability to directly control shape, chemistry and interconnected porosity of the printed structure: in fact, 3DP is based on an additive process where successive layers of one or more materials are laid down onto the previous ones and stacked into different pre-programmed shapes [49,50]. Finally, the 3D object is obtained as the sum of many 2D printed layers [49,51]. Polymers are especially well-suited for this approach as they can be used in liquid or solid phase and in different forms, such as solutions of monomers, thermoplastic filaments, powders or resins. Among the numerous polymers tested, the most commonly used are poly (lactic acid) (PLA), acrylonitrile–butadienestyrene (ABS), polycarbonate (PC), polyamides, polycaprolactone (PCL) and polystyrene [51]. The main advantages of their use are related to the ease of their processing and manufacturing. In addition, polymers chemical flexibility allows their derivatization with multiple functional groups [50,52].

In this work, we describe the synthesis of a photo-crosslinkable pullulan derivative that can be exploited in 3D printing processes for the construction of three-dimensional structures. In this view, methacrylate groups have been introduced along the polysaccharide backbone by an esterification reaction. The product is investigated in terms of functionalization and cross-linking degree with a multi-technique approach (^{1}H NMR and ^{13}C NMR, FT-IR and Raman spectroscopy). The self-assembly properties in water have been investigated by phase-contrast optical microscopy (PCM) and Small Angle Scattering of X-Rays (SAXS), as well as the rheological behavior. This is especially relevant for the printability of the dispersions that were tested in a 3D inkjet printer, also in presence of UV rays to activate the cross-linking. The process parameters (such as printing speed, layer thickness, needle gauge, fill density) were optimized and the obtained printouts were evaluated in terms of their structure by means of AFM and of their tensile properties to evaluate the effects of functionalization and cross-linking.

2. Materials and methods

2.1. Materials

Pullulan, manufactured by Hayashibara Co., Ltd. (Japan), was kindly provided by Giusto Faravelli S.p.A (Milan, Italy). Methacrylic anhydride (MA, 2000 ppm Topanol A as inhibitor, 94%) and sodium hydroxide (NaOH, pellets, 97+ %) were obtained from Sigma-Aldrich (Milan, Italy). Ethanol (EtOH, absolute denatured ≥ 99.2% (v/v)) was purchased from Carlo Erba (Milan, Italy). All reagents were used without any further purification. Demineralized H_2O was used as reaction solvent and for preparation of printing solutions. 2-Hydroxy-4′-(2-hydroxyethoxy)-2-methylpropiophenone (IRGACURE 2959, 98%), obtained from Sigma-Aldrich (Milan, Italy), was chosen as radical photo-initiator for photo-polymerization process. Sodium Azide (NaN_3) was obtained from Sigma-Aldrich (Milan, Italy) and used to avoid degradation in pullulan solutions.

2.2. Methacrylated pullulan synthesis

Methacrylated pullulan (Pul-Ma) was synthetized following the procedure reported by Della Giustina et al. [53]. Briefly, pullulan (Pul) was dissolved under stirring at room temperature (RT) in water (2.5% w/v). The solution was cooled down to 4 °C. MA was slowly added up to a concentration of 0.5% v/v continuously adjusting the pH at 8 by adding NaOH 10 M. The solution was stirred at 4 °C for 24 h. The product was precipitated from ethanol to remove unreacted methacrylic anhydride, ground with a blender to facilitate ethanol evaporation, centrifuged and dried under vacuum to obtain a white solid stored at 4 °C.

2.3. Nuclear magnetic resonance spectroscopy (^{1}H NMR, ^{13}C NMR)

^{1}H NMR and ^{13}C NMR spectra of Pul and Pul-Ma were recorded, respectively, in D_2O and DMSO d_6 with a Bruker Advance III spectrometer operating at 400 MHz Larmor frequency for the

proton, using the signal of the solvent residual protons as internal reference. The functionalization degree (FD), defined as the ratio of methacrylate groups with respect to maltotriose units of pullulan, was calculated by ^{1}H NMR spectrum of Pul-Ma by using the following relation (Eq. (1)):

$$FD = \frac{I_{1.90ppm}}{I_{4.02-3.35ppm}} * 6 \quad (1)$$

where $I_{1.90\ ppm}$ is the integrated area of the methyl group peak and $I_{4.02\text{-}3.35\ ppm}$ is the integrated area of non-anomeric protons signals of pullulan.

2.4. Fourier transform infrared spectroscopy (FT-IR)

FT-IR analyses of the lyophilized powders were performed with a Nexus 870 FT-IR spectrophotometer equipped with an ATR (Attenuated Total Reflectance) Golden Gate accessory. Spectra were recorded at RT within the wavenumber range of 4000–650 cm^{-1} (128 scans and with a spectral resolution of 2 cm^{-1}).

2.5. Photo-polymerization

IRGACURE 2959, a radical photo-initiator working in the UV spectral region, was dissolved in an aqueous solution of Pul-Ma (30% w/w). The concentration of IRGACURE 2959 in the obtained sample, labelled as Pul-MAUV, is 0.79% molar compared to methacrylate groups present in solution. Once fully dissolved, the solution was irradiated with an LSH102 UV mercury-vapor lamp provided with an optic fiber and connected to a Lot Oriel LSN150 power supply operating at 130 Watt.

2.6. Raman confocal microscopy

Raman spectroscopy has been used to evaluate the photo-polymerization process. Raman spectra of Pul, Pul-Ma and Pu-MaUV (powders) have been acquired with a InVia^{TM} Rehishaw microscope using a 100 × lens and a near-infrared laser operating at 785 nm.

2.7. Phase-contrast microscopy (PCM)

Optical images of aqueous solutions of Pul and Pul-Ma (concentration 30% w/w) have been obtained with a Nikon Diaphot 300 phase-contrast microscope equipped with a 20x lens. Digital images were acquired with a CCD (Charge-Coupled Device) Digital Sight DS-U1 Nikon.

2.8. Small Angle X-rays scattering (SAXS)

SAXS experiments were carried out with a HECUS SWAX camera (Kratky) equipped with a position-sensitive detector (OED 50 M) containing 1024 channels of width 54 μm. Cu Kα radiation of wavelength k = 1.542 Å was provided by a Seifert ID-3003 X-rays generator (sealed-tube type), operating at a maximum power of 2 kW (50 kV and 1 mA). All the scattering curves were recorded in the q-range between 0.012 and 0.55 $Å^{-1}$. A small quantity of each sample was sealed in a cell between two Kapton windows. Scattering curves were corrected for the water and Kapton contributions. The data were analyzed with SasView software (http://www.sasview.org/).

2.9. Rheology

Rheological measurements were carried out with a Discovery HR3 Hybrid rheometer (TA Instrument) using a plate-plate geometry (top plate diameter 2 cm) with a distance between plates (geometry gap) of 300 μm and using a torque range of 0.01–1000 μN·m. All measurements were performed on aqueous solutions of Pul and Pul-Ma with a concentration of 30% (w/w) at RT, recording 10 points for decade with soak and duration time of 300 s and 600 s respectively.

2.10. 3D printing

3D objects, labelled as 3Dfilms, were produced using an HYREL 3D Engine SR injection 3D printer and an SDS-10 syringe head equipped with an electric motor. The 3Dfilms were printed on a glass printing bed heated at 68 °C. Aqueous solutions (added with NaN_3 in trace amounts when stored before printing) of Pul and Pul-Ma at the concentration of 30% w/w were tested for 3D printing without UV radiation as a reference material. An apparent viscosity value of 3.4 Pa·s of these solutions during the printing process was estimated from the Poiseuille law, taking into account the geometrical parameters of the syringe and the needle used and the axial force applied by the electric motor of the printing head (see Supplementary Material, Equation S1). Photo-initiator IRGACURE 2959 was added to a Pul-Ma solution (concentration 30% w/w) at a specific concentration (0.79% compared to methacrylic units present in solution). This sample has been irradiated during the printing with a UV lamp to induce the cross-linking of methacrylic groups (see Materials and Methods). To obtain that, the 3D printer head was integrated with an optic fiber irradiating the ejected material close to the tip of the needle. The processing parameters used for the printing are shown in Table 1.

2.11. Atomic force microscopy (AFM)

A XE7 AFM (Park System) was used to image the sample. The samples were scanned in non-contact mode with NCHR probes (radius of curvature of the tip around 5 nm) at room temperature. All scans were recorded as 512 pixels × 512 pixels images. The roughness profile of samples surface over 25 μm^2 areas were evaluated according to the RMS roughness R_q which is the standard deviation of the height value in a specific region and it's calculated by the following equation:

$$R_q = \sqrt{\frac{1}{n}\sum_{i=1}^{n}\left(z_i - z_{avg}\right)^2} \quad (2)$$

where z_{avg} is the average height value calculated over the n pixels and z_i is the height of the i-th pixel.

2.12. Mechanical tests

Uniaxial tensile tests were performed on 3Dfilms of 10 mm × 40 mm × 0.6 mm (length × width × thickness). All measurements were carried out using a Discovery HR3 Hybrid rheometer (TA Instrument), equipped with a Film Tension

Table 1
3D printing processing parameters.

Parameter	Value	Parameter	Value
Needle outer diameter	0.7 mm	Flow	(9.31–3.07) *10^{-4} mL/s
Needle inner diameter	0.4 mm	*Needle Gauge*	G22
Fill density	100%	*Fill pattern*	Rectilinear
Object dimension	10 mm × 40 mm × 0.6 mm	*Speed*	1 mm/s
Layer thickness	0.2 mm	*First layer thickness*	0.15 mm

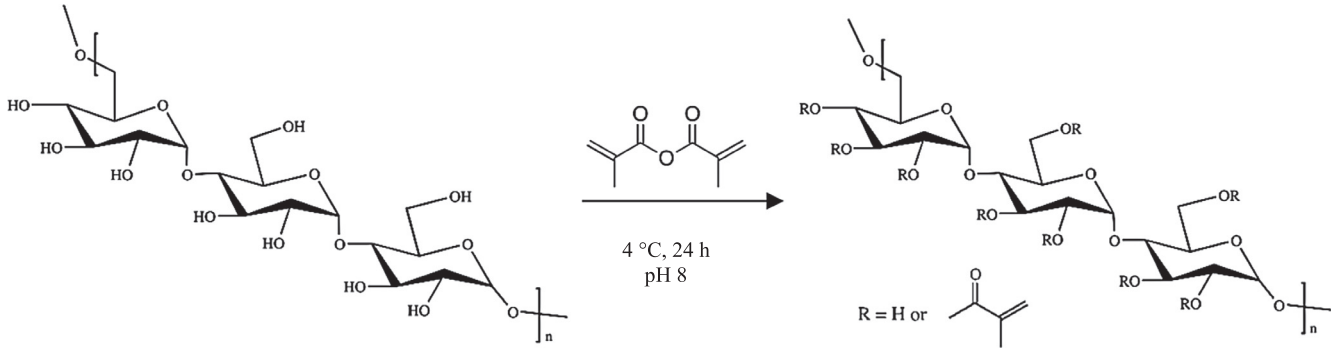

Fig. 1. Reaction scheme for the synthesis of methacrylated pullulan (Pul-MA).

Dynamic Mechanical Analysis tool. The following parameters were used: initial gap 2 cm, speed to rupture 94 μm/s. All data obtained have been reported as applied axial force vs percentage of elongation, which has been calculated as (Eq. (3)):

$$Elongation(\%) = \frac{l_i(\mu m) - l_0(\mu m)}{l_0(\mu m)} * 100 \quad (3)$$

where l_i is the gap measured by the instrument at the i-th point and l_0 is the initial gap. The yield point, the breaking load, the elongation at break and stiffness, calculated as the angular coefficients in the linear range of elastic deformation in the axial force vs percentage of elongation graphs, were evaluated.

3. Results and discussion

3.1. Pul-Ma synthesis, characterization and photo-polymerization

The esterification reaction between methacrylic anhydride and the hydroxyl groups of the glucopyranose residues leads to the introduction of methacrylate units along the polysaccharide backbone (Fig. 1), as confirmed by NMR and FT-IR analyses. In general, the functionalization may occur in all the position of the pyranose ring, but the C6 position is the most probable due to lower steric hindrance. Fig. 2a shows the Pul-Ma ^{1}H NMR spectrum recorded in D_2O. Proton signals observed in the region 3.35–4.02 ppm and at δ 4.90 and 5.32 ppm correspond to non-anomeric and anomeric protons of pullulan, respectively. The signals at δ 5.72 and 6.15 ppm can be assigned to the hydrogens of the C=C double bonds, while the peak at δ 1.91 ppm to the methyl protons of the methacrylate group. The corresponding signals can be observed in the ^{13}C NMR spectrum of Pul-Ma (Fig. 2b). Beside the characteristic peaks of the maltotriose unit of pullulan (C1 about 101.43–98.77 ppm, C4 at 80.85 ppm and 80.03 ppm, C6 around 67.03–60.29 ppm and *C*2,3,5 between 73.43 and 70.08 ppm), the ^{13}C NMR spectrum exhibits the methacrylate functional group signals: at 171.80 ppm for the carbonyl group, at 144.30 ppm and 117.54 ppm for the C=C group and at 20.08 ppm for the methyl group. The functionalization degree (FD), defined as the ratio of methacrylate groups with respect to maltotriose units of pullulan, obtained by ^{1}H NMR analysis is about 0.27 (corresponding to a concentration of 0.53 mmol/g). FT-IR spectroscopy investigations confirm the presence of methacrylate groups on pullulan chains: in fact, as shown in Fig. 3, along with absorption peaks attributed to pullulan [22,54,55,56,57,58], FT-IR spectrum of Pul-Ma shows a peak at 1709 cm^{-1}, which is characteristic of the stretching of carbonyl groups of methacrylate moieties [43,59].

The photo-polymerization process (see Materials and Methods) is based on a free radical polymerization process between methacrylate groups, using IRGACURE 2959 as the photo-initiator in the UV spectral region (maximum absorbance at 276 nm) [60].

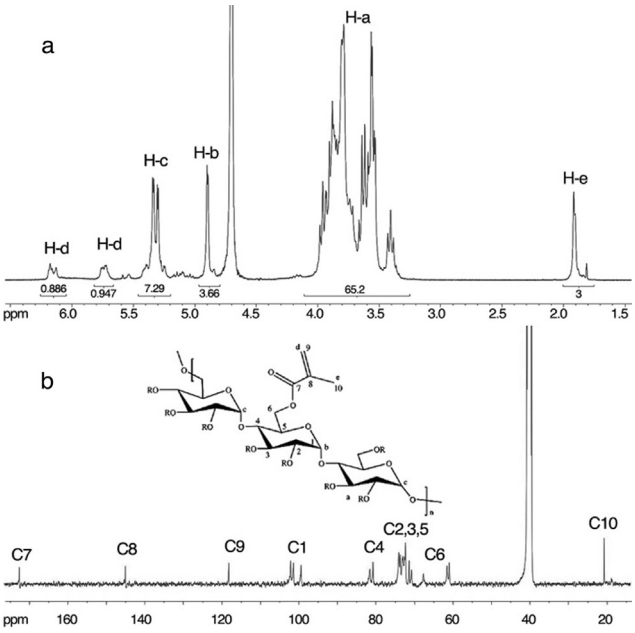

Fig. 2. ^{1}H NMR spectrum of Pul-Ma in D_2O (a) and ^{13}C NMR of Pul-Ma in DMSO d_6 (b).

The cross-linking of pullulan chains results in a marked change of the solubility of the product: Pul-Ma is soluble in water and dimethyl sulfoxide (DMSO), while the irradiated sample (Pul-MaUV) does not dissolve in these solvents, even after several days. The effective photo-polymerization of Pul-Ma was verified by Raman spectroscopy. The spectra reported in Fig. 4 have been normalized using the peak at 1461 cm^{-1}, as this signal (attributed to CH_2 bending) is expected to remain nearly constant in all the samples. The signals at 1638 cm^{-1} and 1710 cm^{-1} observed in Pul-Ma and Pul-MaUV, but not in Pul spectrum, are attributed to C=C and C=O stretching, which are characteristic of the presence of unreacted methacrylic groups [61]. The comparison between the intensity of the C=C stretching peaks in Pul-Ma and Pul-MaUV shows a clear decrease, thus confirming that the cross-linking has taken place.

3.2. Self-assembly properties

Even though Pul and Pul-Ma water solutions appear macroscopically homogenous up to very high concentrations (up to 40% w/w), optical microscopy investigations revealed the presence of aggregates at the micro-scale in both samples. Dynamic light scattering experiments (data not shown) have shown the formation of micro-

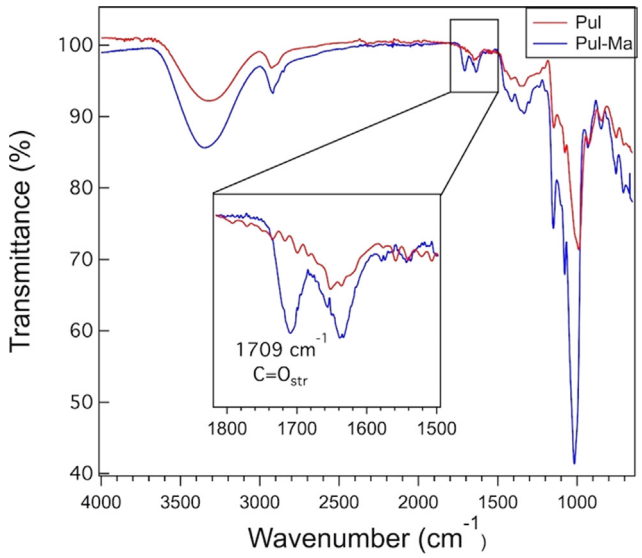

Fig. 3. FT-IR spectra of Pul (red) and Pul-Ma (blue). (For interpretation of the references to colour in this figure legend, the reader is referred to the web version of this article.)

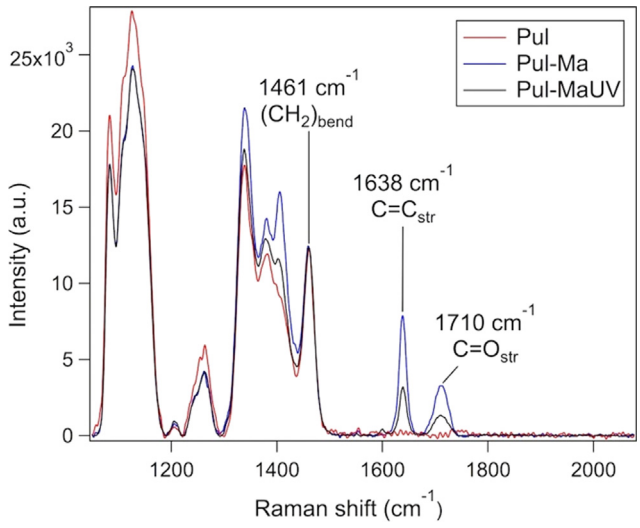

Fig. 4. Raman spectra of Pul (red), Pul-Ma (blue) and Pul-MaUV (black). All the spectra were normalized using the peak at 1461 cm^{-1}. (For interpretation of the references to colour in this figure legend, the reader is referred to the web version of this article.)

metric aggregates already at concentrations below 5% w/w. At a concentration of 30% w/w, which was selected for the printing experiments, phase-contrast optical microscopy (Fig. 5) shows the presence of micrometric polysaccharide aggregates dispersed in water having similar size regardless of the composition.

SAXS was used to shed light on the structure of these aggregates down to the nanoscale. SAXS curves of Pul and Pul-Ma in water (Fig. 6) were fitted using the Polydisperse Gaussian coils model [62–64] that can be used to model polydisperse polymer chains in good solvents. The total scattering intensity *I(q)* is described by the following equation:

$$I(q) = scale \cdot I_0 \cdot P(q) + background \tag{4}$$

where:

$$I_0 = \phi_{poly} \cdot V \cdot (\rho_{poly} - \rho_{solv})^2 \tag{5}$$

$$P(q) = 2\left[(1+UZ)^{-1/U} + Z - 1\right] / \left[(1+U)Z^2\right] \tag{6}$$

$$Z = \left[(qR_g)^2\right] / (1+2U) \tag{7}$$

$$U = (M_w/M_n) - 1 \tag{8}$$

$$V = M/(N_A\delta) \tag{9}$$

where ϕ_{poly} is the volume fraction of polymer, V is the polymer coil volume, M is the polymer molecular weight, N_A is the Avogadro's number, δ is the bulk density of the polymer, R_g is the radius of gyration of the polymer coil, ρ_{poly} and ρ_{solv} are the scattering length densities of the polymer and the solvent, respectively. The polydispersity value was kept equal to 2 since pullulan is characterized by a number-average molecular weight (M_n) value between 100 e 200 kDa and a weight-average molecular weight (M_w) about 362–480 kDa [13]. The gyration radius (R_g) values obtained from the fitting for Pul and Pul-Ma are reported with the corresponding errors in Table 2. The results are consistent with those obtained with the Polymer Excluded-Volume model [65–68], also reported in Table 2. This model describes the scattering intensity in term of polymer chains subjected to excluded volume effects, using the following relation for the form factor *P(q)*:

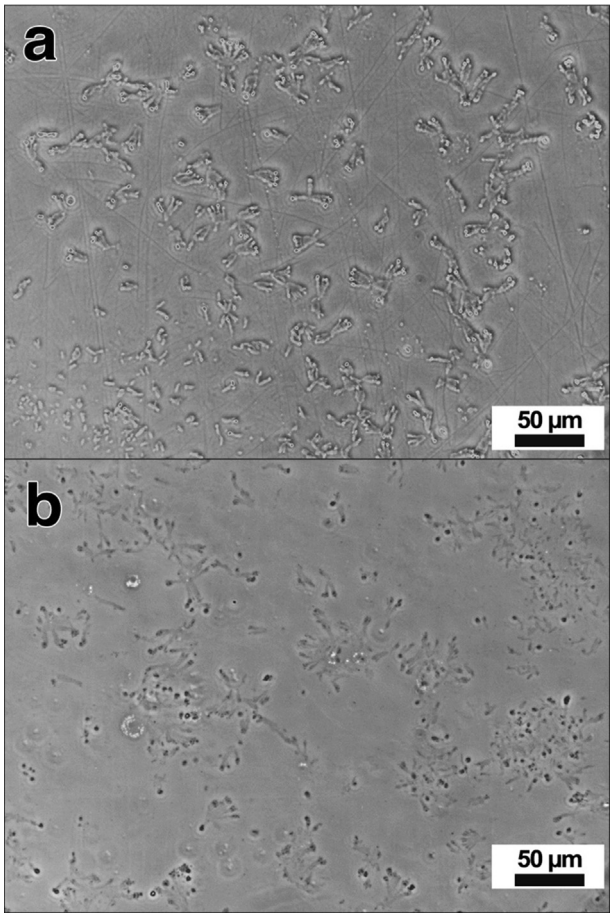

Fig. 5. Phase-contrast optical images of Pul (**a**) and Pul-Ma (**b**) aqueous solutions at 30% (w/w).

$$P(q) = \frac{1}{vU^{1/2v}}\gamma\left(\frac{1}{2v}, U\right) - \frac{1}{vU^{1/v}}\gamma\left(\frac{1}{v}, U\right) \tag{10}$$

where $\gamma(x,U)$ is the incomplete gamma function:

$$\gamma(x,U) = \int_0^U dt \exp(-t)t^{x-1} \tag{11}$$

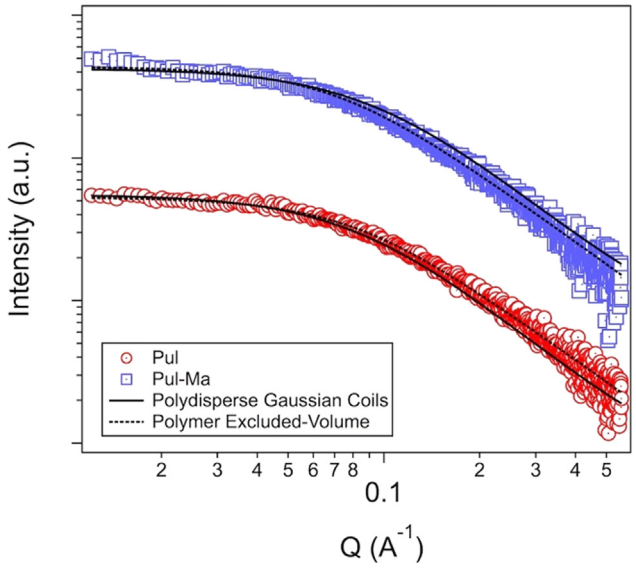

Fig. 6. SAXS curve of Pul (red curve) and Pul-Ma (blue curve) aqueous solution at 30% (w/w) and relative fittings. Curves are vertically offset for clarity of presentation. (For interpretation of the references to colour in this figure legend, the reader is referred to the web version of this article.)

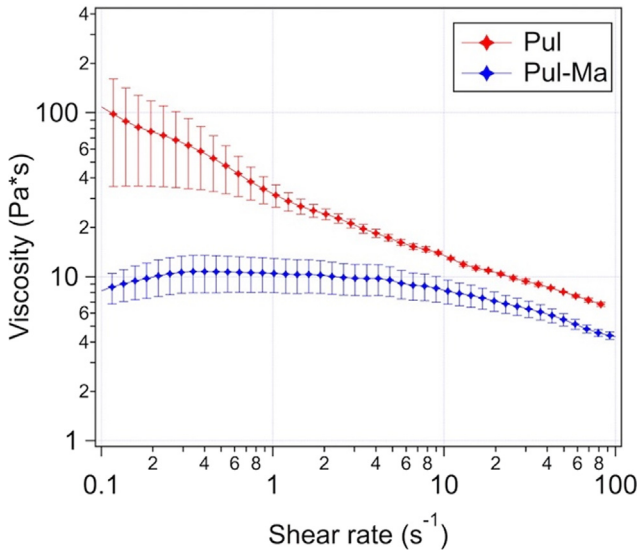

Fig. 7. Viscosity curve of aqueous solutions of Pul (red) and Pul-Ma (blue) at 30% w/w. (For interpretation of the references to colour in this figure legend, the reader is referred to the web version of this article.)

Table 2
Parameters obtained from the fitting of SAXS curves of Pul and Pul-Ma 30% w/w in water.

Sample	Model fitting	R_g (Å)	Polydispersity	Porod exponent
Pul	Polymer_excl_volume	16.6 ± 0.1	/	1.62 ± 0.01
	Poly_Gauss_coil	17.3 ± 0.1	2	/
Pul-Ma	Polymer_excl_volume	18.8 ± 0.1	/	1.64 ± 0.01
	Poly_Gauss_coil	19.5 ± 0.1	2	/

and the variable U is a function of the scattering vector q, defined as:

$$U = \frac{q^2 a^2 n^{2\nu}}{6} = \frac{q^2 R_g^2 (2\nu+1)(2\nu+2)}{6} \quad (12)$$

Here, ν is the excluded volume, a is the statistical segment length of the polymer chain and n is the polymerization degree. The use of this model allows to obtain the Porod exponent (m), which is related to the inverse of the excluded volume term ($m = 1/\nu$) and provides information about the fractal dimension of the scattering objects. An exponent $m = 1.6$ is found for both samples (Table 2) and it is a signature of fully swollen coils [69].

SAXS results suggest that the micrometric aggregates observed by PCM consist of swollen pullulan coils having a R_g below 2 nm and highlight that the functionalization with methacrylic groups does not dramatically affect the self-assembly properties of pullulan, producing a slight increase of R_g for Pul-Ma which could be related to the hindrance introduced by the lateral functions along the polymer chain, eventually resulting in a less interpenetrated coil structure.

The self-assembly properties of Pul and Pul-Ma in water were investigated in terms of their rheological behavior, also in view of their printing. Viscosity curves of Pul and Pul-Ma water dispersions (30% w/w) are reported in Fig. 7 (the corresponding flow curves are given in the Supplementary Material, Figure S1). It is worth noting that the lower viscosity of highly concentrated pullulan aqueous solutions compared to other polysaccharides highlights the low tendency of pullulan molecules to self-assemble in water. Pul sample shows a non-Newtonian behavior throughout the entire investigated shear rate range (0.1–100 s^{-1}), with a nearly constant shear-thinning trend. Pul-Ma sample displays a lower viscosity compared to Pul. Furthermore, a region at low shear rates where the viscosity remains nearly constant (often referred to as a Newtonian plateau) is present, followed by a shear-thinning behavior. Highly concentrated polysaccharide solutions are well known to behave as interpenetrated polymer coils and react to external deformations as dynamically entangled network structures [70]. At low shear rates, the deformation breaks the existing entanglements, which are quickly replaced by newly formed ones, resulting in a Newtonian plateau. At increasing shear rates, when the rate of formation of new entanglements is not sufficient to replace the ones disrupted by the deformation, the net degree of interpenetration decreases and the system shows a shear-thinning behavior. In our case, the results suggest that the presence of methacrylic groups on the side chains leads to a decrease of the total number of entanglements, as the viscosity of Pul-Ma is lower than that of Pul, consistently with SAXS results. This behavior is especially evident at lower shear rates, where Pul sample shows a significantly higher viscosity. In view of the 3D printing, the introduction of methacrylic groups does not dramatically change the rheological properties of pullulan; nevertheless, the presence of a Newtonian plateau could be of help in providing a stable and reliable flow at low shear rates, *i.e.*, at low printing speed.

3.3. Printing

In this work we used an injection 3D printer to obtain a polymeric object with a parallelepiped shape and dimensions of 10 mm × 40 mm × 0.6 mm using aqueous solutions of pullulan and methacrylated pullulan (with and without IRGACURE 2959) at the concentration of 30% w/w. Images of the printed 3Dfilms have been reported in Figure S2 in the Supplementary Material. The use of a heated printing bed was chosen so to promote solvent evaporation and solidification of the printed polymeric solution. Bed temperature, and consequently evaporation time, along with printing speed are the main parameters to optimize the layer by layer process and the development along the third axis

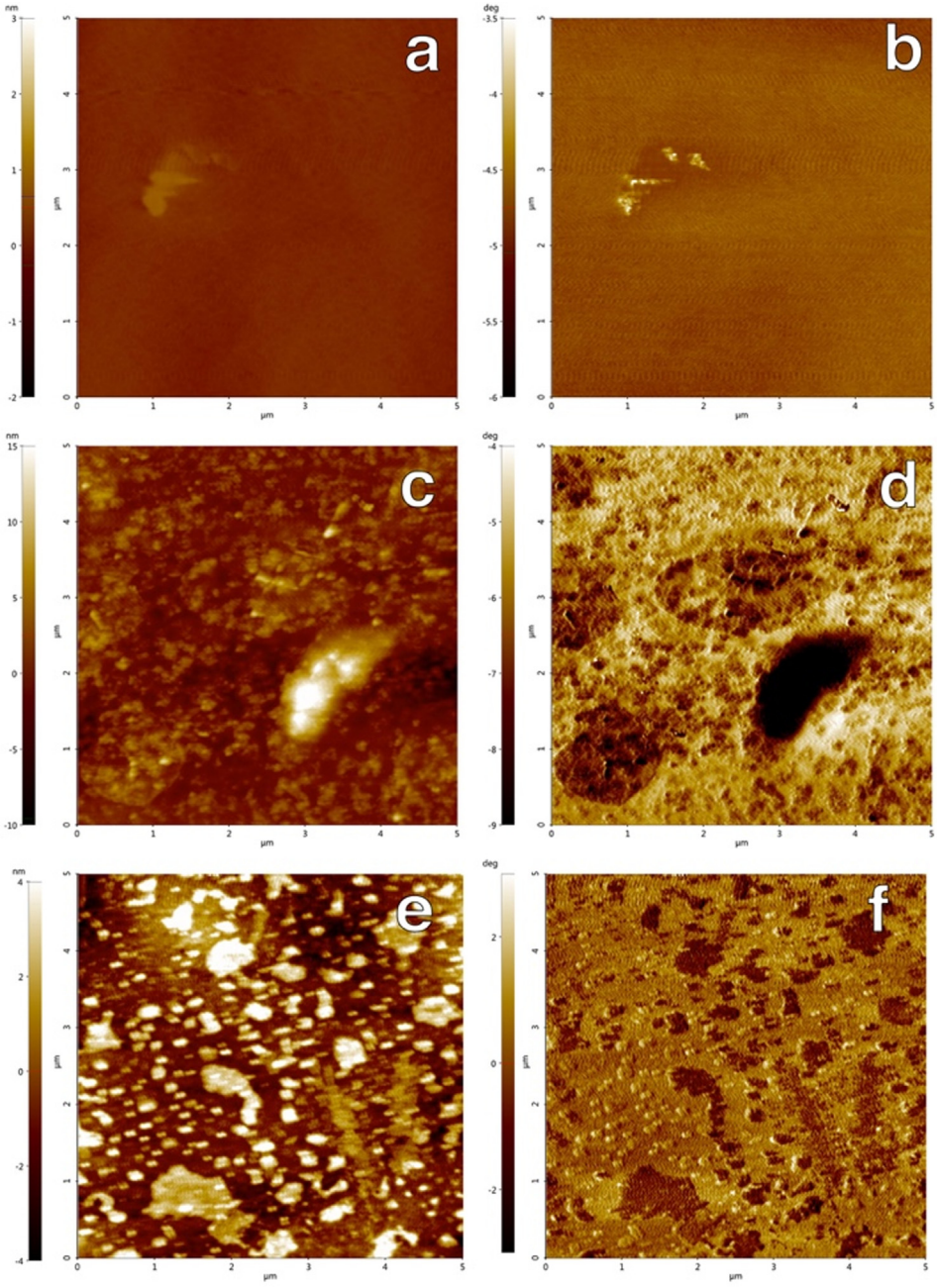

Fig. 8. AFM topography and phase images of Pul (a and b, respectively), Pul-Ma (c and d, respectively) and Pul-MaUV (e and f, respectively).

(z): in fact, the printing speed and bed temperature are set so that the *n + 1* layer will be deposited on the *n* layer only when this is partly solidified. The fill density (%) parameter is the percentual ratio between the space occupied by the solid polymeric material and the empty space in the final structure, eventually defining the porosity of the printed object. The fill pattern parameter describes the series of movements performed by the printer head to fill the structure. A rectilinear fill pattern and a fill density 100% were chosen for all the samples. Using the same pattern allowed us to compare 3D printed films in terms of the material used as the ink. Due to the temperature of the printing bed (68 °C), the proximity of the needle could cause the solvent to evaporate not only from the material on the bed, but also from that in the tip of the needle, potentially leading to inhomogeneous flows. This phenomenon could eventually be amplified when UV is used to activate the cross-linking, especially if the radiation is not confined to the printed material. In our setup, the proper confinement was obtained by using an optical fiber to focus the UV radiation on the immediate proximity of the tip of the needle. Using a G22 needle, irregular flow was observed using printing speeds of 0.2 mm/s or slower. To guarantee an even flow of the material, we used a printing speed of 1 mm/s for all the tested inks (*i.e.*, Pul, Pul-Ma and Pul-MaUV), resulting in the successful production of free-standing films with pre-programmed shape and dimension for all the tested inks. When stored in relatively dry conditions (relative humidity below 50%), no signs of enzymatic degradation of the printed samples were detected. These results highlight that both pullulan and methacrylated pullulan, with and without the cross-linking step, are printable with an extrusion printer.

Table 3
Obtained parameters from tensile tests and AFM analyses of Pul, Pul-Ma and Pul-MaUV 3Dfilms.

Sample	Breaking load (N)	Elongation at break (%)	Yield point y axis (N)	Yield point x axis (%)	Stiffness (N/%)	R_q (nm)
Pul	> 40	1.25 ± 0.12	32.5 ± 3.2	0.60 ± 0.06	45.3 ± 4.5	0.8 ± 0.08
Pul-Ma	24.5 ± 2.4	1.82 ± 0.18	19.7 ± 2.0	1.10 ± 0.11	18.7 ± 1.9	2.4 ± 0.24
Pul-MaUV	5.8 ± 0.6	2.42 ± 0.24	4.9 ± 0.5	2.15 ± 0.21	4.0 ± 0.4	1.8 ± 0.18

3.4. Morphology and mechanical properties of printed films

Printed samples were investigated by Atomic Force Microscopy in non-contact mode to evaluate both the structure and the roughness of the surface. As illustrated in Fig. 8a, Pul 3Dfilms show a homogeneous and smooth surface, as suggested by the phase image (Fig. 8b) and by the very low roughness ($R_q \approx 0.8$ nm). On the other hand, Pul-Ma samples (Fig. 8c and 8d) show the presence of segregated domains with size in the order of few tens of nanometers and a rougher surface ($R_q \approx 2.4$ nm). The surface of Pul-MaUV samples (Fig. 8e and 8f) is similar to Pul-Ma, except for the better definition of the segregated domains and the slightly lower roughness ($R_q \approx 1.8$ nm), consistently with the cross-linked structure. The results suggest that the introduction of methacrylic groups takes to a phase segregation of the submicrometric domains that are further segregated when chemically cross-linked.

3Dfilms were tested to evaluate the effects of the functionalization and the consequent polymerization on their mechanical properties, especially on their tensile strength. Samples were subjected to an increasing applied force while recording their elongation to evaluate the breaking load, the yield point, the angular coefficient and the elongation at break. The resulting values (calculated as described in the Supplementary Material, Figure S3) are shown in Table 3. Pul sample exhibits a tensile strength (*i.e.*, the breaking load value) that exceeds the maximum value allowed by our instrumental setup (40 N). The introduction of methacrylic groups reduces the breaking load to 24.5 N, which further reduces to 5.8 N after the cross-linking. The Stiffness (calculated as the angular coefficient in the linear region) and the yield stress (*i.e.*, the stress at which the elastic behavior is lost) show an analogous trend, while the elongation at break displays an inverted trend.

Correlating these results with the structural information found by AFM suggests that the homogeneous and well-ordered Pul samples behave as a brittle material, with a high value of breaking load and low ability to extend/deform. The introduction of methacrylic groups on the pullulan backbone leads to a less homogeneous structure, with phase segregated domains, resulting in a decrease of the tensile properties of the material. The photo-polymerization process further enhances the differences between the pristine and the functionalized pullulan, producing a material with lower resistance towards applied stresses but enhanced ability to deform before breaking.

4. Conclusions

In this work, we successfully synthetized a photo-crosslinkable pullulan derivative (Pul-Ma) thanks to the introduction of methacrylic functionalities along the polysaccharide chains. The derivative was characterized by means of NMR, FT-IR and Raman spectroscopy. The self-assembly properties of the pristine pullulan and of its derivative in water (30 %w/w) were investigated by means of phase-contrast microscopy and Small Angle Scattering of X-rays, showing that the polymer forms micrometric structures consisting of hydrated polymer chains assembled into swollen coils. The rheological properties were studied in view of using the aqueous dispersions as inks for 3D printing, showing that the typical rheological behavior of polysaccharides (*i.e.*, behaving as interpenetrated polymer coils, able to react to external deformations as dynamically entangled networks) is preserved in the methacrylated derivative. The 3D printing of the aqueous dispersions of pristine and functionalized polymers was optimized in terms of the processing parameter, producing self-standing printouts that were characterized by means of AFM and for their tensile properties. Results highlight that the functionalization and, to a larger extent, the photo-polymerization lead the formation of sub-micrometric segregated domains, most reasonably because of the spatial concentration of methacrylic units, inducing a drastic decrease of the tensile strength and an increase of the extent of deformation allowed by the material.

The results reported in this paper clearly show that pullulan can be functionalized so to feature the required characteristics for being 3D printed into scaffolds, which could be stabilized both by solvent evaporation and by photo-polymerization. We extended the applicability of aqueous solution of Pul and Pul-Ma to inkjet 3D printing techniques, since similar materials have been previously tested only for visible stereolithography (SL) process and two photon lithography (TPL) [53]. In this framework, injection printing allows for shorter printing times and higher flexibility on printable architectures. These results pave the way to the use of pullulan and its derivatives in applications that require a spatial and structural control of the final products. In view of an eventual future use of this material in biomedical applications, the increase of the functionalization degree, *i.e.*, the number of photo-active units, and its effects on structural properties should be investigated. The ability to program and predict the architecture, both in terms of internal porosity and external shape, opens up several possibilities for the realization of specific and complex objects, which are difficult to obtain with other techniques.

CRediT authorship contribution statement

Giulia Mugnaini: Conceptualization, Methodology, Formal analysis, Investigation, Writing - original draft, Writing - review & editing, Visualization. **Claudio Resta:** Formal analysis, Investigation, Writing - original draft. **Giovanna Poggi:** Formal analysis, Investigation, Writing - original draft. **Massimo Bonini:** Conceptualization, Methodology, Formal analysis, Writing - original draft, Writing - review & editing, Visualization, Supervision, Project administration, Funding acquisition.

Declaration of Competing Interest

None.

Acknowledgement:

CSGI and Fondazione Cassa di Risparmio di Firenze are acknowledged for financial support. This work benefited from the use of the SasView application, originally developed under NSF award DMR-0520547. SasView contains code developed with funding from the European Union's Horizon 2020 research and innovation programme under the SINE2020 project, grant agreement No 654000.

Appendix A. Supplementary data

Supplementary data to this article can be found online at https://doi.org/10.1016/j.jcis.2021.02.074.

References:

[1] M. Bonini, Physico-Chemical Challenges in 3D Printing of Polymeric Nanocomposites and Hydrogels for Biomedical Applications, J. Nanosci. Nanotechnol. 21 (2021) 2778–2792. https://doi.org/10.1166/jnn.2021.19063.

[2] H. Mittal, S.S. Ray, B.S. Kaith, J.K. Bhatia, J. Sharma Sukriti, S.M. Alhassan, Recent Progress in the Structural Modification of Chitosan for Applications in Diversified Biomedical Fields, Eur. Polymer J. 109 (2018) 402–434. https://doi.org/10.1016/j.eurpolymj.2018.10.013.

[3] C. Intini, L. Elviri, J. Cabral, S. Mros, C. Bergonzi, A. Bianchera, L. Flammini, P. Govoni, E. Barocelli, R. Bettini, M. McConnell, 3D-Printed Chitosan-Based Scaffolds: An in Vitro Study of Human Skin Cell Growth and an in-Vivo Wound Healing Evaluation in Experimental Diabetes in Rats, Carbohydr. Polym. 199 (2018) 593–602, https://doi.org/10.1016/j.carbpol.2018.07.057.

[4] Q. Zhang, D. Lin, S. Yao, Review on Biomedical and Bioengineering Applications of Cellulose Sulfate, Carbohydr. Polym. 132 (2015) 311–322, https://doi.org/10.1016/j.carbpol.2015.06.041.

[5] K. Markstedt, A. Mantas, I. Tournier, H. Martínez Ávila, D. Hägg, P. Gatenholm, 3D Bioprinting Human Chondrocytes with Nanocellulose-Alginate Bioink for Cartilage Tissue Engineering Applications, Biomacromolecules 16 (5) (2015) 1489–1496, https://doi.org/10.1021/acs.biomac.5b00188.

[6] K. Su, C. Wang, Recent Advances in the Use of Gelatin in Biomedical Research, Biotechnol. Lett. 37 (11) (2015) 2139–2145, https://doi.org/10.1007/s10529-015-1907-0.

[7] K. Yue, G. Trujillo-de Santiago, M.M. Alvarez, A. Tamayol, N. Annabi, A. Khademhosseini, Synthesis, Properties, and Biomedical Applications of Gelatin Methacryloyl (GelMA) Hydrogels, Biomaterials 73 (2015) 254–271, https://doi.org/10.1016/j.biomaterials.2015.08.045.

[8] M.C. Echave, P. Sánchez, J.L. Pedraz, G. Orive, Progress of Gelatin-Based 3D Approaches for Bone Regeneration, J. Drug Delivery Sci. Technol. 42 (2017) 63–74, https://doi.org/10.1016/j.jddst.2017.04.012.

[9] T. Billiet, E. Gevaert, T. De Schryver, M. Cornelissen, P. Dubruel, The 3D Printing of Gelatin Methacrylamide Cell-Laden Tissue-Engineered Constructs with High Cell Viability, Biomaterials 35 (1) (2014) 49–62, https://doi.org/10.1016/j.biomaterials.2013.09.078.

[10] R.S. Singh, N. Kaur, V. Rana, J.F. Kennedy, Recent Insights on Applications of Pullulan in Tissue Engineering, Carbohydr. Polym. 153 (2016) 455–462, https://doi.org/10.1016/j.carbpol.2016.07.118.

[11] J. Li, C. Wu, P.K. Chu, M. Gelinsky, 3D Printing of Hydrogels: Rational Design Strategies and Emerging Biomedical Applications, Mater. Sci. Eng.: R: Rep. 140 (2020), https://doi.org/10.1016/j.mser.2020.100543 100543.

[12] K.I. Shingel, Current Knowledge on Biosynthesis, Biological Activity, and Chemical Modification of the Exopolysaccharide, Pullulan, Carbohydr. Res. 339 (3) (2004) 447–460, https://doi.org/10.1016/j.carres.2003.10.034.

[13] R.S. Singh, G.K. Saini, J.F. Kennedy, Pullulan: Microbial Sources, Production and Applications, Carbohydr. Polym. 73 (4) (2008) 515–531, https://doi.org/10.1016/j.carbpol.2008.01.003.

[14] R.S. Singh, N. Kaur, J.F. Kennedy, Pullulan and Pullulan Derivatives as Promising Biomolecules for Drug and Gene Targeting, Carbohydr. Polym. 123 (2015) 190–207, https://doi.org/10.1016/j.carbpol.2015.01.032.

[15] S. Tabasum, A. Noreen, M.F. Maqsood, H. Umar, N. Akram, Z.-H. Nazli, S.A.S. Chatha, K.M. Zia, A Review on Versatile Applications of Blends and Composites of Pullulan with Natural and Synthetic Polymers, Int. J. Biol. Macromol. 120 (2018) 603–632, https://doi.org/10.1016/j.ijbiomac.2018.07.154.

[16] B. Bernier, The Production of Polysaccharides by Fungi Active in the Decomposition of Wood and Forest Litter, Can. J. Microbiol. 4 (3) (1958) 195–204, https://doi.org/10.1139/m58-020.

[17] H. Bender, K. Wellenfels, Investigations on Pullulan. II. Specific Degradation by Means of a Bacterial Enzyme, Biochem. Zeitschrift 334 (1961) 79–95.

[18] K. Wallenfels, G. Keilich, G. Bechtler, D. Freudenberger, Investigations on Pullulan. IV. Resolution of Structural Problems Using Physical, Chemical and Enzymatic Methods, Biochemische Zeitschrift 341 (1965) 433–450.

[19] V. Trinetta, C.N. Cutter, Chapter 30 - Pullulan: A Suitable Biopolymer for Antimicrobial Food Packaging Applications, in: J. Barros-Velázquez, Ed. Antimicrobial Food Packaging Academic Press: San Diego, 2016, pp 385–397. https://doi.org/10.1016/B978-0-12-800723-5.00030-9.

[20] T.D. Leathers, Biotechnological Production and Applications of Pullulan, Appl. Microbiol. Biotechnol. 62 (5–6) (2003) 468–473, https://doi.org/10.1007/s00253-003-1386-4.

[21] G.A. Morris, G.G. Adams, S.E. Harding, On Hydrodynamic Methods for the Analysis of the Sizes and Shapes of Polysaccharides in Dilute Solution: A Short Review, Food Hydrocolloids 42 (2014) 318–334, https://doi.org/10.1016/j.foodhyd.2014.04.014.

[22] S. Farris, L. Introzzi, J.M. Fuentes-Alventosa, N. Santo, R. Rocca, L. Piergiovanni, Self-Assembled Pullulan-Silica Oxygen Barrier Hybrid Coatings for Food Packaging Applications, J. Agric. Food Chem. 60 (3) (2012) 782–790, https://doi.org/10.1021/jf204033d.

[23] S. Farris, I.U. Unalan, L. Introzzi, J.M. Fuentes-Alventosa, C.A. Cozzolino, Pullulan-Based Films and Coatings for Food Packaging: Present Applications, Emerging Opportunities, and Future Challenges, J. Appl. Polym. Sci. 131 (13) (2014), https://doi.org/10.1002/app.40539.

[24] M. Dionísio, C. Cordeiro, C. Remuñán-López, B. Seijo, A.M. Rosa da Costa, A. Grenha, Pullulan-Based Nanoparticles as Carriers for Transmucosal Protein Delivery, Eur. J. Pharm. Sci. 50 (1) (2013) 102–113, https://doi.org/10.1016/j.ejps.2013.04.018.

[25] Y. Han, S. Lv, Synthesis of Chemically Crosslinked Pullulan/Gelatin-Based Extracellular Matrix-Mimetic Gels, Int. J. Biol. Macromol. 122 (2019) 1262–1270, https://doi.org/10.1016/j.ijbiomac.2018.09.080.

[26] I. Bataille, A. Meddahi-Pellé, C. Le Visage, L. Didler, F. Chaubet, Chapter 4-Pullulan for Biomedical Uses, in: Polysaccharides in Medicinal and Pharmaceutical Applications; iSmithers, 2011; pp 145–182.

[27] N. Teramoto, M. Shibata, Synthesis and Properties of Pullulan Acetate. Thermal Properties, Biodegradability, and a Semi-Clear Gel Formation in Organic Solvents, Carbohydr. Polym. 63 (2006) 476–481, https://doi.org/10.1016/j.carbpol.2005.10.008.

[28] Y. Tezuka, Pullulan Nonaacetate: Assignment of Chemical Shifts of the Acetyl Protons and Acetyl Carbonyl Carbons by 2D-NMR Spectroscopy, Carbohydr. Res. 305 (2) (1997) 155–161, https://doi.org/10.1016/S0008-6215(97)10036-2.

[29] D. Bruneel, E. Schacht, Chemical Modification of Pullulan: 1. Periodate Oxidation, Polymer 34 (12) (1993) 2628–2632, https://doi.org/10.1016/0032-3861(93)90600-F.

[30] A.E.J. de Nooy, M. Pagliaro, H. van Bekkum, A.C. Besemer, Autocatalytic Oxidation of Primary Hydroxyl Functions in Glucans with Nitrogen Oxides, Carbohydr. Res. 304 (2) (1997) 117–123, https://doi.org/10.1016/S0008-6215(97)10004-0.

[31] A. Spatareanu, M. Bercea, T. Budtova, V. Harabagiu, L. Sacarescu, S. Coseri, Synthesis, Characterization and Solution Behaviour of Oxidized Pullulan, Carbohydr. Polym. 111 (2014) 63–71, https://doi.org/10.1016/j.carbpol.2014.04.060.

[32] G. Mocanu, D. Mihai, L. Picton, D. LeCerf, G. Muller, Associative Pullulan Gels and Their Interaction with Biological Active Substances, J. Control. Release 83 (1) (2002) 41–51, https://doi.org/10.1016/S0168-3659(02)00169-4.

[33] L. Picton, G. Mocanu, D. Mihai, A. Carpov, G. Mullera, Chemically Modified Exopolysaccharide Pullulans: Physico-Chemical Characteristics of Ionic Derivatives, Carbohydr. Polym. 28 (2), 131–136.

[34] S. Wu, Z. Jin, J.M. Kim, Q. Tong, H. Chen, Graft Copolymerization of Methyl Acrylate onto Pullulan Using Ceric Ammonium Nitrate as Initiator, Carbohydr. Polym. 76 (1) (2009) 129–132, https://doi.org/10.1016/j.carbpol.2008.10.002.

[35] D. Bontempo, G. Masci, P. De Leonardis, L. Mannina, D. Capitani, V. Crescenzi, Versatile Grafting of Polysaccharides in Homogeneous Mild Conditions by Using Atom Transfer Radical Polymerization, Biomacromolecules 7 (7) (2006) 2154–2161, https://doi.org/10.1021/bm0601373.

[36] S. Belbekhouche, G. Ali, V. Dulong, L. Picton, D. Le Cerf, Synthesis and Characterization of Thermosensitive and Ph-Sensitive Block Copolymers Based on Polyetheramine and Pullulan with Different Length, Carbohydr. Polym. 86 (1) (2011) 304–312, https://doi.org/10.1016/j.carbpol.2011.04.053.

[37] M. Dionísio, L. Braz, M. Corvo, J.P. Lourenço, A. Grenha, A.M. Rosa da Costa, Charged Pullulan Derivatives for the Development of Nanocarriers by Polyelectrolyte Complexation, Int. J. Biol. Macromol. 86 (2016) 129–138, https://doi.org/10.1016/j.ijbiomac.2016.01.054.

[38] G. Mocanu, M. Costantin, A. Carpov, Chloroacetylated Derivatives of Dextran. Chemical Reactions on Polysaccarides. 5. Reaction of Mesyl Chloride with Pullulan. 241 (1996) 1–10.

[39] M.F. Akhtar, M. Hanif, N.M. Ranjha, Methods of Synthesis of Hydrogels A Review, Saudi Pharmaceut. J. 24 (5) (2016) 554–559, https://doi.org/10.1016/j.jsps.2015.03.022.

[40] R. Gauvin, Y.C. Chen, J.W. Lee, P. Soman, P. Zorlutuna, J.W. Nichol, H. Bae, S. Chen, A. Khademhosseini, Microfabrication of Complex Porous Tissue Engineering Scaffolds Using 3D Projection Stereolithography, Biomaterials 33 (15) (2012) 3824–3834, https://doi.org/10.1016/j.biomaterials.2012.01.048.

[41] N. Morimoto, T. Endo, M. Ohtomi, Y. Iwasaki, K. Akiyoshi, Hybrid Nanogels with Physical and Chemical Cross-Linking Structures as Nanocarriers, Macromol. Biosci. 5 (8) (2005) 710–716, https://doi.org/10.1002/mabi.200500051.

[42] W.N.E. van Dijk-Wolthuis, O. Franssen, H. Talsma, M.J. van Steenbergen, J.J. Kettenes-van den Bosch, W.E. Hennink, Synthesis, Characterization, and Polymerization of Glycidyl Methacrylate Derivatized Dextran, Macromolecules 28 (18) (1995) 6317–6322. https://doi.org/10.1021/ma00122a044.

[43] G. Masci, D. Bontempo, V. Crescenzi, Synthesis and Characterization of Thermoresponsive N-Isopropylacrylamide/Methacrylated Pullulan Hydrogels, Polymer 43 (20) (2002) 5587–5593, https://doi.org/10.1016/S0032-3861(02)00415-9.

[44] I.A. de Lima, S.P. Pomin, O.A. Cavalcanti, I.A. de Lima, S.P. Pomin, O.A. Cavalcanti, Development and Characterization of Pullulan-Polymethacrylate Free Films as Potential Material for Enteric Drug Release, Brazil. J. Pharmaceut. Sci, 53 (3) (2017). https://doi.org/10.1590/s2175-97902017000300002.

[45] P. Ferreira, P. Santos, P. Alves, M.P. Carvalho, K.D. de Sá, S.P. Miguel, I.J. Correia, P. Coimbra, Photocrosslinkable Electrospun Fiber Meshes for Tissue Engineering Applications, Eur. Polym. J. 97 (2017) 210–219, https://doi.org/10.1016/j.eurpolymj.2017.10.018.

[46] D. Atila, D. Keskin, A. Tezcaner, Crosslinked Pullulan/Cellulose Acetate Fibrous Scaffolds for Bone Tissue Engineering, Mater. Sci. Eng. C-Mater. Biol. Appl. 69 (2016) 1103–1115, https://doi.org/10.1016/j.msec.2016.08.015.
[47] L.K. Vora, A.J. Courtenay, I.A. Tekko, E. Larrañeta, R.F. Donnelly, Pullulan-Based Dissolving Microneedle Arrays for Enhanced Transdermal Delivery of Small and Large Biomolecules, Int. J. Biol. Macromol. 146 (2020) 290–298, https://doi.org/10.1016/j.ijbiomac.2019.12.184.
[48] D.F.S. Fonseca, P.C. Costa, I.F. Almeida, P. Dias-Pereira, I. Correia-Sá, V. Bastos, H. Oliveira, M. Duarte-Araújo, M. Morato, C. Vilela, A.J.D. Silvestre, C.S.R. Freire, Pullulan Microneedle Patches for the Efficient Transdermal Administration of Insulin Envisioning Diabetes Treatment, Carbohydr. Polym. 116314 (2020), https://doi.org/10.1016/j.carbpol.2020.116314.
[49] X. Li, R. Cui, L. Sun, K.E. Aifantis, Y. Fan, Q. Feng, F. Cui, F. Watari, 3D-Printed Biopolymers for Tissue Engineering Application https://www.hindawi.com/journals/ijps/2014/829145/abs/ (accessed Mar 28, 2019). https://doi.org/10.1155/2014/829145.
[50] S. Bose, S. Vahabzadeh, A. Bandyopadhyay, Bone Tissue Engineering Using 3D Printing, Mater. Today 16 (12) (2013) 496–504, https://doi.org/10.1016/j.mattod.2013.11.017.
[51] T.D. Ngo, A. Kashani, G. Imbalzano, K.T.Q. Nguyen, D. Hui, Additive Manufacturing (3D Printing): A Review of Materials, Methods, Applications and Challenges, Compos. B Eng. 143 (2018) 172–196, https://doi.org/10.1016/j.compositesb.2018.02.012.
[52] S.F.S. Shirazi, S. Gharehkhani, M. Mehrali, H. Yarmand, H.S.C. Metselaar, N. Adib Kadri, N.A.A. Osman, A Review on Powder-Based Additive Manufacturing for Tissue Engineering: Selective Laser Sintering and Inkjet 3D Printing, Sci. Technol. Adv. Mater. 16 (3) (2015), https://doi.org/10.1088/1468-6996/16/3/033502 033502.
[53] G. Della Giustina, A. Gandin, L. Brigo, T. Panciera, S. Giulitti, P. Sgarbossa, D. D'Alessandro, L. Trombi, S. Danti, G. Brusatin, Polysaccharide Hydrogels for Multiscale 3D Printing of Pullulan Scaffolds, Mater. Des. 165 (2019), https://doi.org/10.1016/j.matdes.2018.107566 107566.
[54] K.I. Shingel, Determination of Structural Peculiarities of Dexran, Pullulan and γ-Irradiated Pullulan by Fourier-Transform IR Spectroscopy, Carbohydr. Res. 337 (16) (2002) 1445–1451, https://doi.org/10.1016/S0008-6215(02)00209-4.
[55] S. Saber-Samandari, O. Gulcan, S. Saber-Samandari, M. Gazi, Efficient Removal of Anionic and Cationic Dyes from an Aqueous Solution Using Pullulan-Graft-Polyacrylamide Porous Hydrogel, Water Air Soil Pollut. 225 (2014) 2177, https://doi.org/10.1007/s11270-014-2177-5.
[56] R.S. Singh, G.K. Saini, Pullulan-Hyperproducing Color Variant Strain of Aureobasidium Pullulans FB-1 Newly Isolated from Phylloplane of Ficus Sp, Bioresour. Technol. 99 (9) (2007) 3896–3899, https://doi.org/10.1016/j.biortech.2007.08.003.
[57] K.C. Cheng, A. Demirci, J.M. Catchmark, Effects of Plastic Composite Support and PH Profiles on Pullulan Production in a Biofilm Reactor, Appl. Microbiol. Biotechnol. 86 (3) (2010) 853–861, https://doi.org/10.1007/s00253-009-2332-x.
[58] G.V. Salmoria, P. Klauss, R.A. Paggi, L.A. Kanis, A. Lago, Structure and Mechanical Properties of Cellulose Based Scaffolds Fabricated by Selective Laser Sintering, Polym. Test. 28 (6), 648–652.
[59] H. Bae, A.F. Ahari, H. Shin, J.W. Nichol, C.B. Hutson, M. Masaeli, S.-H. Kim, H. Aubin, S. Yamanlar, A. Khademhosseini, Cell-Laden Microengineered Pullulan Methacrylate Hydrogels Promote Cell Proliferation and 3D Cluster Formation, Soft Matter 7 (5) (2011) 1903–1911, https://doi.org/10.1039/C0SM00697A.
[60] B. Cesur, O. Karahan, S. Agopcan, T.N. Eren, N. Okte, D. Avci, Difunctional Monomeric and Polymeric Photoinitiators: Synthesis and Photoinitiating Behaviors, Prog. Org. Coat. 86 (2015) 71–78, https://doi.org/10.1016/j.porgcoat.2015.04.010.
[61] F. Pallikari, G. Chondrokoukis, M. Rebelakis, Y. Kotsalas, Raman Spectroscopy: A Technique for Estimating Extent of Polymerization in PMMA, Mater. Res. Innovations 4 (2–3) (2001) 89–92, https://doi.org/10.1007/s100190000076.
[62] Small Angle X-Ray Scattering; O. Glatter, O. Kratky, (Eds.); Academic Press, London, New York, 1982.
[63] J.S. Higgins, H. Benoît, *Polymers and Neutron Scattering*; Oxford series on neutron scattering in condensed matter, Clarendon Press; Oxford University Press, Oxford, New York, 1994.
[64] Modern Techniques for Polymer Characterisation; R.A. Pethrick, J.V. Dawkins (Eds.); J. Wiley: Chichester, West Sussex, England, New York, 1999.
[65] H. Benoit, Compte Rendus. 245 (1957) 2244–2247.
[66] B. Hammouda, SANS from Homogeneous Polymer Mixtures: A Unified Overview. In *Polymer Characteristics*; Advances in Polymer Science, Springer-Verlag: Berlin/Heidelberg 106 (1993) 87–133, https://doi.org/10.1007/BFb0025862.
[67] M.J.A. Hore, B. Hammouda, Y. Li, H. Cheng, Co-Nonsolvency of Poly(*n* -Isopropylacrylamide) in Deuterated Water/Ethanol Mixtures, Macromolecules 46 (19) (2013) 7894–7901, https://doi.org/10.1021/ma401665h.
[68] B. Hammouda, M.-H. Kim, The Empirical Core-Chain Model, J. Mol. Liq. 247 (2017) 434–440, https://doi.org/10.1016/j.molliq.2017.09.114.
[69] B. Hammouda, Probing Nanoscale Structures – The Sans Toolbox. <http://www.ncnr.nist.gov/staff/hammouda/the_SANS_toolbox.pdf>.
[70] E.R. Morris, A.N. Cutler, S.B. Ross-Murphy, D.A. Rees, J. Price, Concentration and Shear Rate Dependence of Viscosity in Random Coil Polysaccharide Solutions, Carbohydr. Polym. 1 (1) (1981) 5–21, https://doi.org/10.1016/0144-8617(81)90011-4.